Large Eddy Simulation of Marine Stratocumulus Cloud with Explicit Microphysics

William R. Cotton, Bjorn Stevens, Graham Feingold[1], Robert L. Walko
Colorado State University
Dept. of Atmospheric Science
Fort Collins, CO 80523

ECMWF/GCSS Workshop on Parameterization of the Cloud Topped Boundary Layer,
ECMWF, Reading, United Kingdom, 8-11 June 1993

[1]Affiliation: Cooperative Institute for Research in Environmental Sciences, University of Colorado, Boulder, CO 80309-0449

Abstract

A three dimensional model for simulating the effect of enhanced cloud condensation nucleus concentrations on stratocumulus clouds is presented. The model is a large eddy simulation version of the Regional Atmospheric Modeling System (RAMS) with explicit representation of the cloud condensation nucleus (CCN) spectrum and cloud droplet spectrum. Results of a three-dimensional simulation of the 7 July 1987 FIRE I case is presented.

Horizontally-average profiles of droplet number concentrations are nearly constant through most of the cloud layer, while liquid water content and droplet effective radius increase linearly through the cloud layer. Except near cloud base, average supersaturations remain small; being less than 0.15%.

These results are consistent with both observations and expectations. The only departure from reality is at the grid points near cloud top where supersaturations of the order of 1.3%, unreasonably large liquid water contents, and droplet concentrations about 20% above typical cloud values are found. These anomalies are numerical artifacts resulting from non-monotonic advection.

1. Introduction

Twomey (1974, 1977) hypothesized that increased anthropogenic sources of aerosol will result in the presence of greater numbers of cloud condensation nuclei (CCN) which will produce higher concentrations of cloud droplets, and, consequently, more reflective clouds. This effect is believed to have the greatest impact on optically thin marine stratocumulus clouds. It has also been suggested (Albrecht, 1989) that enhanced CCN concentrations will suppress the rate of formation of drizzle drops. This will result in a positive feedback into the CCN-albedo link since reduced drizzle in clouds with higher drop concentrations, will result in larger liquid water paths, and, hence, more reflective clouds. Recently Charlson *et al.* (1992) estimated that a 15% increase in global mean droplet concentrations in marine stratus and stratocumulus clouds results in a radiative cooling effect comparable (and opposite in sign) to current estimates of greenhouse warming.

Before this hypothesis can be placed on a sound scientific basis it is necessary to quantify the sensitivity of cloud albedo to CCN concentrations in particular cloud types. The final goal of our research is to provide quantitative estimates of this sensitivity for the special case of marine stratocumulus clouds and to develop a parameterization scheme of boundary

layer clouds suitable for use in general circulation models (GCMs) that contains explicit dependence upon CCN concentrations.

Our approach is to introduce an explicit cloud microphysics scheme into the Regional Atmospheric Modeling System (RAMS) developed at Colorado State University. The RAMS is configured as a large eddy simulation (LES) model in which the major energy-containing eddies are explicitly resolved. Model simulations will produce a large cloud microphysics/macrophysics data base which will then be used by a sophisticated radiative transfer model to evaluate the impacts on cloud albedo.

The aim of this paper is three-fold: (i) to present the RAMS model in its new configuration with explicit microphysics; and (ii) to examine the credibility of the combined explicit microphysics/LES model. In Section 2 we describe the design and implementation of the LES version of RAMS and the explicit microphysics model. In Section 3 we present results from a three-dimensional large eddy simulation (LES) using a sounding from a stratocumulus case observed during FIRE I. Section 4 presents a discussion of the results.

2. Model Description

a. *RAMS as an LES model*

The RAMS is a multi-purpose modeling system that has been applied to LES over inhomogeneous land surfaces (Hadfield *et al.*, 1991, 1992; Walko *et al.*, 1992) and to the simulation of a variety of cloud systems. In this investigation RAMS is set up as a non-hydrostatic LES model. Prognostic equations include those for the three velocity components (u, v, w), liquid water potential temperature (θ_l; Tripoli and Cotton, 1981), perturbation Exner function π, and total water mixing ratio r_t (the sum of vapor and liquid water mixing ratios). In all previous cloud applications a bulk microphysical scheme, which diagnoses cloud liquid water (*e.g.*, Cotton *et al.*, 1986), has been used. In the current explicit microphysics model, condensate is predicted using a droplet spectrum which we resolve into 25 different size bins. Prognostic equations are required for each of these bins and the liquid water mixing ratio r_l is the sum of the mixing ratios in each bin. In RAMS, water vapor mixing ratio r_v

is diagnosed as the difference between the total mixing ratio r_t and the liquid water mixing ratio r_l. Temperature T is diagnosed from the prognostic variables θ_l and r_l. This enables calculations of cloud supersaturation S:

$$S = \frac{r_v}{r_s(T)} - 1 = \frac{r_t - r_l}{r_s(T)} - 1, \tag{1}$$

where $r_s(T)$ is the saturation mixing ratio calculated from polynomial fits to saturation vapor pressure and the diagnosed temperature T (Flatau *et al.*, 1992). In calculating S, both the dynamical and microphysical tendencies are accounted for. Tests of the stability of this calculation to model time step show only weak sensitivity for a doubling of the time step from 1 s to 2 s (Cotton *et al.*, 1992).

A further modification of RAMS has been the addition of a positive definite scheme for the advection of microphysical variables. The advection schemes operate in a hybrid mode with vector quantities (u, v, w) advected using a fourth order leap-frog scheme, while liquid water substances and other scalar quantities are advected using a positive definite, sixth order forward differencing scheme. The positive definite scheme employs the flux limitations of Bott (1989), within the framework of the higher order polynomial fits of Tremback *et al.*, (1987).

The model includes explicit feedback of bulk cloud properties on radiative heating/cooling based on the radiation parameterization developed by Chen and Cotton (1983). Sub-grid scale diffusion is parameterized using a Smagorinsky deformation tensor modified for stability. The lower boundary condition is a surface layer parameterization based on the Louis (1979) scheme, with specified sea surface temperatures. The top boundary is a rigid lid with the option of a Rayleigh friction wave-absorbing layer in the top most grid points. Lateral boundary conditions are specified as cyclic. We have the option of spawning a sequence of finer grids which will allow us to study various processes (such as cloud top entrainment) with increasingly finer resolutions.

b. *The explicit microphysics model*

The explicit microphysics model that has been implemented in RAMS is an accurate moment-conserving scheme developed by the Tel-Aviv University Cloud Physics Group. Tzivion *et al.* (1987) showed that the accuracy of this method in representing condensation and collection is comparable to that of schemes which use two to three times the number of bins, but predict on only the mass concentration in each bin (*e.g.*, Bleck, 1970). For stratocumulus simulations, a total of 25 bins characterize a drop spectrum in the range 1.56 – 504 μm (radius), with mass doubling from one bin to the next. Since we are primarily concerned with non-precipitating stratocumulus clouds and clouds with only light amounts of drizzle, the specified size range should be adequate. The microphysical processes affecting the drop spectrum are droplet activation from CCN, condensation/evaporation, collision-coalescence, and sedimentation. Drop breakup is not considered as it is expected to be negligible for these clouds. Because the 25 bins are represented by both mass and number mixing ratio we require 50 prognostic equations for the drop spectrum variables.

Coupling the explicit microphysics with the dynamical model required the development of a droplet activation scheme. Our approach was based on a 6 bin representation of the CCN distribution in supersaturation space (i.e., CCN were divided on the basis of their observed activation supersaturation, see Table 1). The nucleation scheme is a modified version Twomey's (1959) generic formula:

$$N_a = Cs^K,$$

where s is the supersaturation in percent, and C and K are empirically determined constants. Using measurements of Hudson and Frisbie (1991) we account for an apparent supersaturation dependence of K, and let C vary according to the number of CCN dynamically present. Thus we define a fractional activation spectra for the case that $S_{min,i-1} > s > S_{min,i}$

$$N_{a,i} = N_{t,i}\left[f(s) - f(s_{min,i})\right],$$

where $f(s) = s^{(k_i \ln s + k_{i0})}$, N_t is the number of dynamically available CCN in bin i, and $K = k_i \ln s + k_{i0}$ represents our empirical fit to the K data of Hudson where k_i and k_{i0} are specified separately for each bin and remain fixed through the course of the simulation.

Table 1: Activation characteristics of the 6 bin CCN distribution. $S_{min,i}$ represents the minimum supersaturation necessary to begin activating CCN residing in bin i. For $S > S_{min,i}$ all the CCN in bins $j > i$ will be activated, so that $S_{min,i} = S_{max,i+1}$.

Bin 1:	$S_{min,1}$ =1.00%	Bin 4:	$S_{min,4}$ = 0.10%
Bin 2:	$S_{min,2}$ =0.60%	Bin 5:	$S_{min,5}$ = 0.02%
Bin 3:	$S_{min,3}$ =0.30%	Bin 6:	$S_{min,6}$ = 0.00%

An advantage of this scheme is that it specifies the CCN field in terms of the critical parameter from which it is measured, activation number is therefore independent of assumptions about chemical species. Furthermore, by defining a distribution within each bin we hope to make the most of the limited information associated with a 6 bin representation of the CCN activation distribution.

Activation size requires assumptions about chemical species, however, this part of the activation process must be parameterized (in multi-dimensional cloud models) to begin with, as the vast majority of CCN commonly activate at a size significantly below the smallest resolved drop. For CCN activating from bin 6 we map to the drop spectra using the 95% size of the corresponding Ammonium Sulfate particles. Two-dimensional results have not shown a sensitivity to this mapping.

When a droplet evaporates completely, it is assumed that one particle is returned to the atmosphere (Mitra *et al.*, 1992). The size distribution of returned aerosols is based upon the relative depletion of the individual bins averaged over the domain. Thus evaporation tends to force the CCN distribution toward its intial state. In 2-D sensitivity tests we have found our simulations to be quite sensitive to the regeneration parameterization, with the above parameterization representing the most stable solution.

Using this scheme we can initiate RAMS with a sounding of CCN and consider vertical and horizontal transport of the CCN by the explicitly represented large eddies. We can

simulate their depletion by activation as well as their replenishment due to droplet evaporation. Moreover, we hope to simulate the interaction between rising plumes of air depleted in CCN and air streams entrained into the cloud containing environmental concentrations of CCN that are characteristic of above-boundary layer air.

By varying the parameters of the initial CCN spectra we can model the preferential activation of larger CCN, and thus better represent the relationship between the spectra of newly activated droplets and that of the available CCN. Also, the possible inclusion of giant nuclei allows us to study their impact on the collision-coalescence process (*e.g.*, Johnson, 1980).

3. Model Configuration and Control Case

As our first test of the combined explicit microphysics model in three-dimensions, RAMS was set up to simulate the well-documented FIRE I case day of 7 July 1987 (e.g., Betts and Boers, 1990).

RAMS was set up as follows:

- Domain of $58 \times 58 \times 36$ points.
- 55 m horizontal grid spacing.
- 25 m vertical grid spacing below 900 m with vertical grid stretching (10–20%) to model top at 2250 m.
- In each horizontal direction 6 grid points are redundant due to 6th order advection scheme with cyclic boundary conditions this leads to an approximately 9 km^2 horizontal domain.
- Rigid lid on top with Rayleigh friction in upper seven levels.
- Winds advected using the fourth order leap-frog scheme of Tremback et al. (1987).
- Radiation scheme of Chen and Cotton (1983).

- Stability modified Smagorinsky subgrid diffusional scheme.
- Model start time specified as 15:30 local time on July 7, 1987.
- Boundary layer sounding taken from Betts & Boers (JAS '90) composite sounding derived from aircraft data for stratocumulus in FIRE observational area July 7, 1987. Mid- and upper-level soundings for use in radiation calculations taken from RAMS interpolation of NMC data.
- CCN initially specified as horizontally homogeneous and matched to spectral measurements of Hudson and Frisbie (1991) for June 29. Concentrations such that approximately 120 per cm^3 activate at supersaturations less than 1%. Taken as a 'typical' marine case.
- Model fields initialized as horizontally homogeneous with random perturbations of surface temperatures not exceeding 0.1 K. Sea surface temperatures taken to be 0.3 K greater than initial air temperatures at lowest levels (*i.e.*, 289.3 K).

Initial model spin up takes approximately 60 minutes, fields are spun up using a 4 second time step, 2nd order advection, collection turned off and radiation calculations every five minutes. The following 140 minutes of simulation was carried out with a 2 second timestep, 6/4th order advection, collection turned on, and radiative calculations every 60 seconds. Domain subjected to a Galilean transform to account for large value of mean winds.

4. Results

a. Domain-averaged fields

We begin by showing the domain-average statistics for the run. Figure 1a illustrates the standard deviation or root mean squared (w_{rms}) in vertical velocity. Following an initial build up during the first 60 minutes, w_{rms} decreases and then exhibits gradual rise until 180 min, where it levels off. Droplet concentrations, on the other hand (see Fig. 1b) become

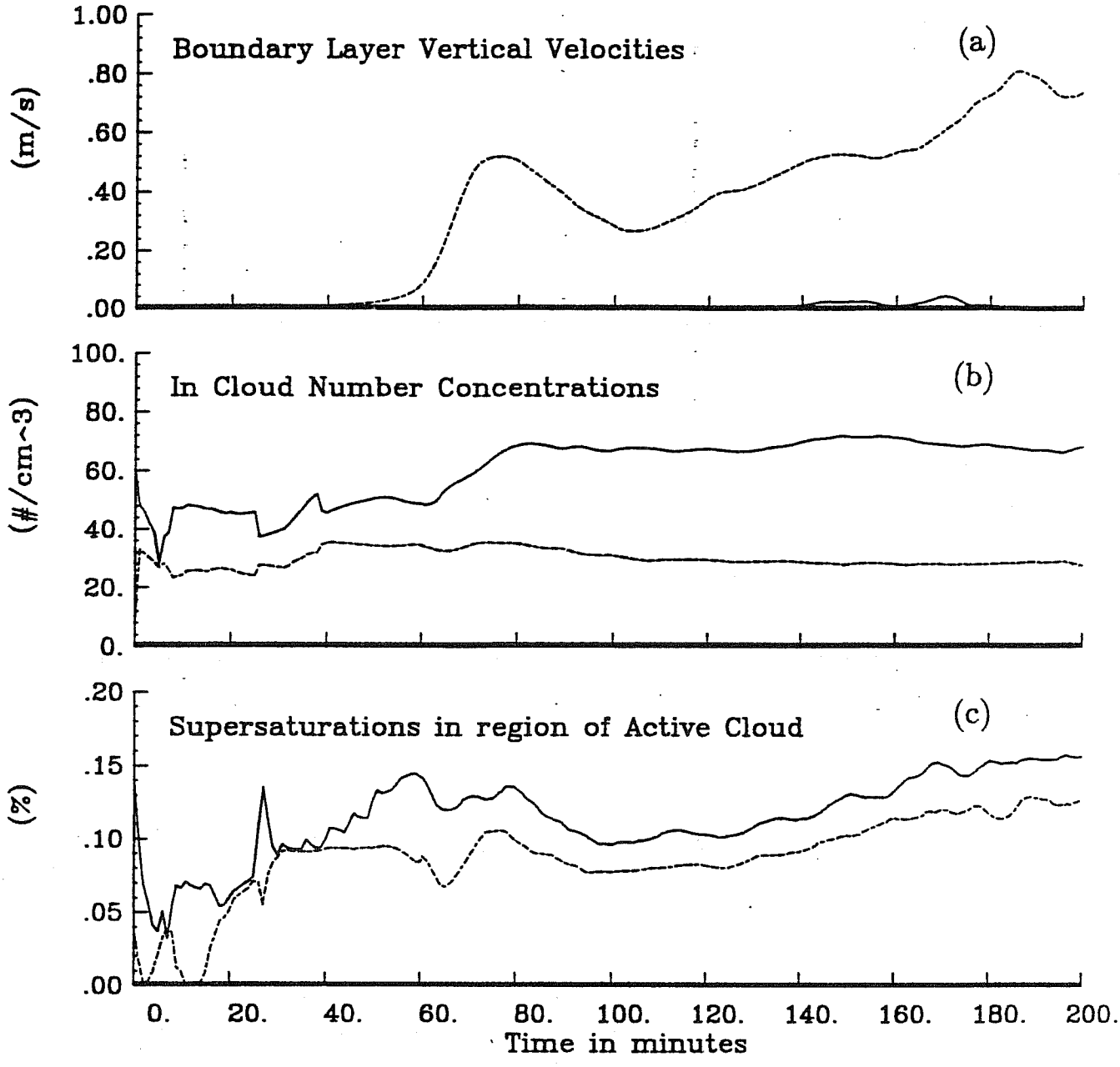

Figure 1: Sub-inversion statistics computed at 30 second intervals over the course of the run. Solid line represents average, dashed lines represent standard deviation or root mean squared (RMS) quantities. (a) vertical velocities; (b) cloud droplet number concentrations; (c) supersaturations averaged in regions where $S > 0$. (d) liquid water contents; (e) liquid water paths; (f) cloud depth; (g) accumulated drizzle (average and standard deviation over surface grid points); (h) drizzle rate (computed from change in accumulated drizzle).

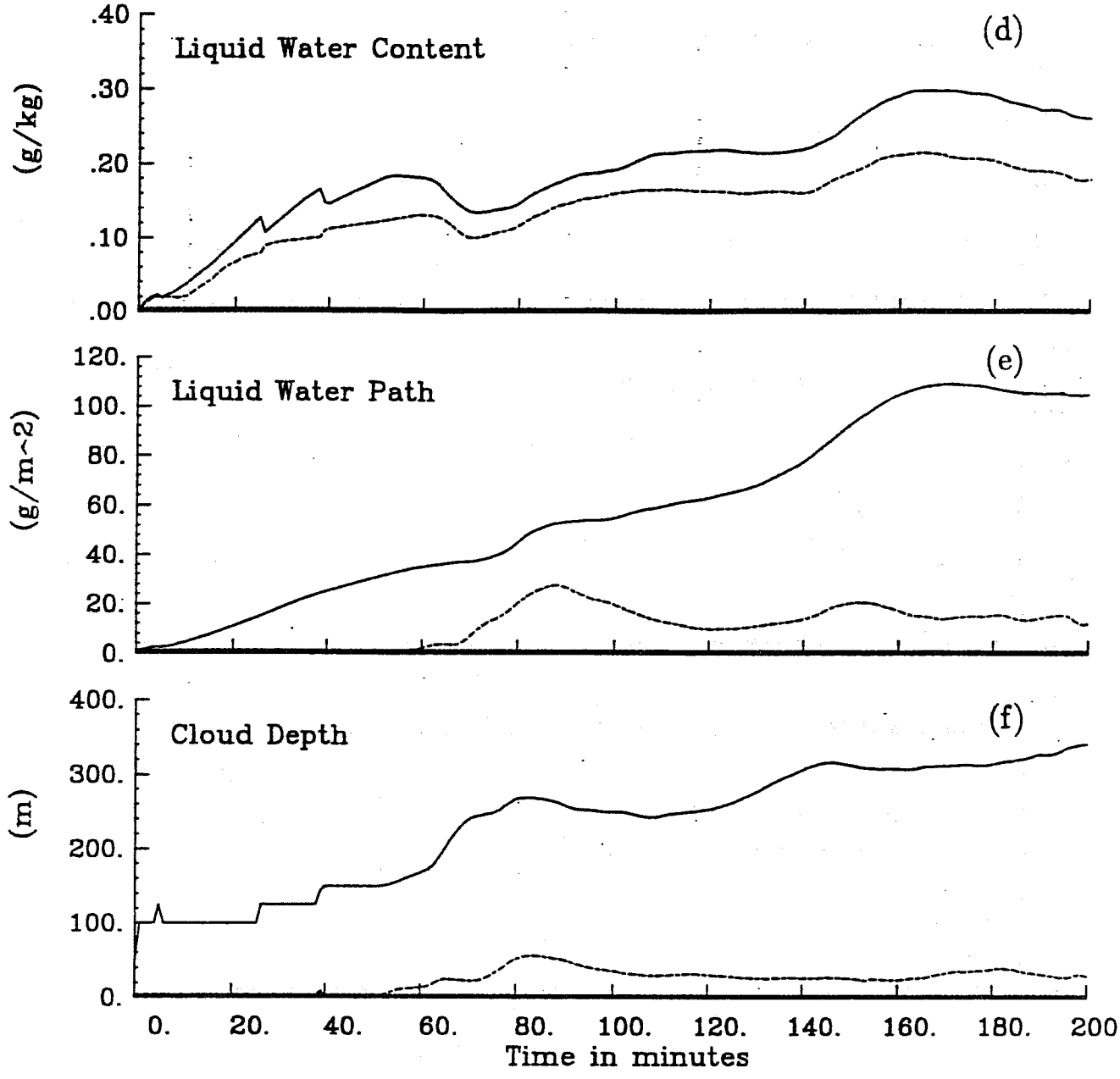

Figure 1: Continued.

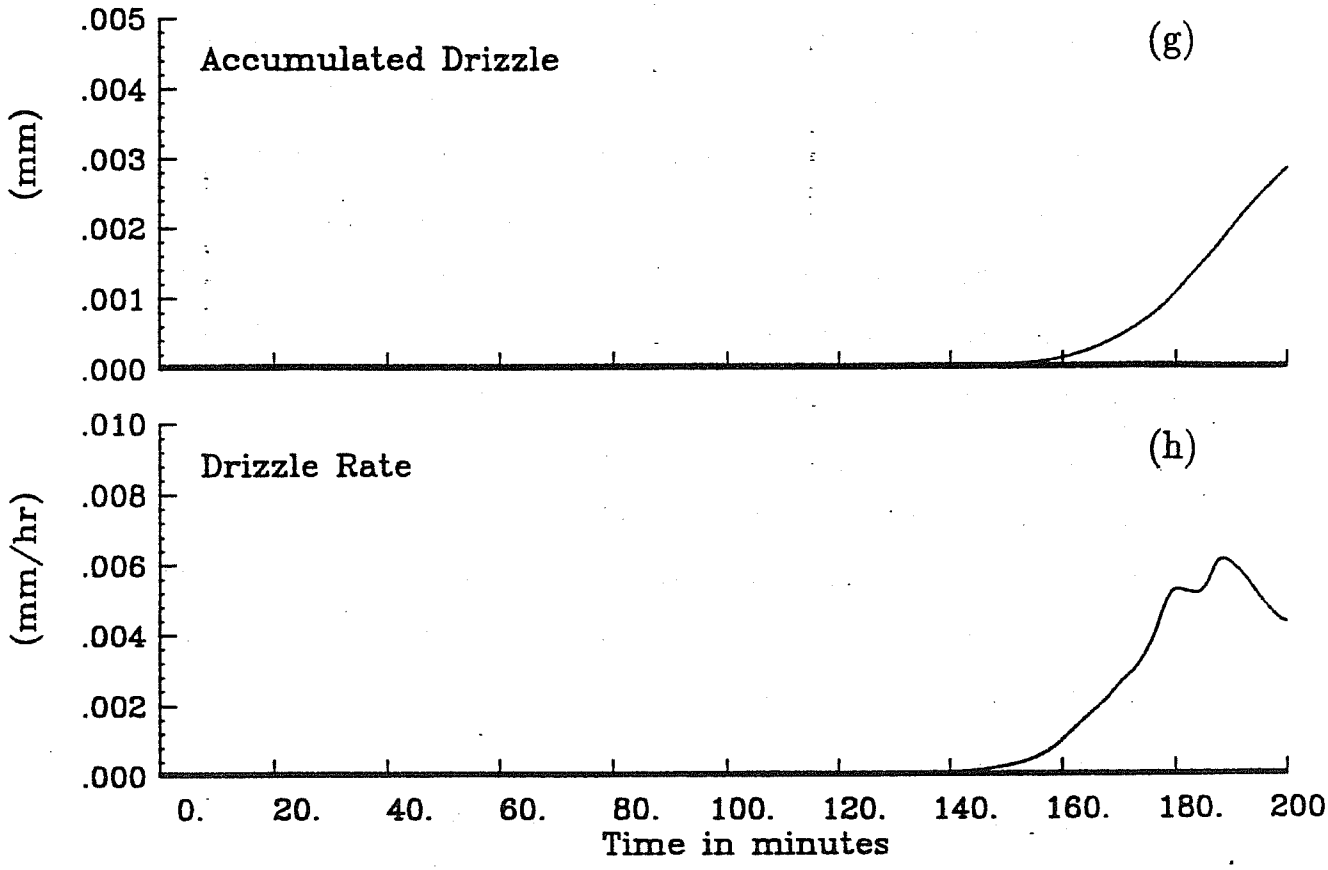

Figure 1: Continued.

steady after only 80 min. Supersaturations (see Fig. 1c) tend to follow w_{rms} with an initial peak at 60 min, followed by a decrease and steady rise to near constant values by 180 min.

Liquid water contents, and to a lesser extent, cloud depth (Fig. 1f) tend to mirror w_{rms} behavior, while liquid water paths (Fig. 1e) exhibits a steady rise until about 165 min. As of yet it has not been conclusively determined to what extent the slow evolution of the liquid water fields is a property of the late afternoon/early evening evolution of the cloud layer vs. a transient respose associated with the numerical integrations. It would be rather disturbing (from a computational cost perspective) if it takes nearly 3 hrs before the domain-average fields become sufficiently steady to carry out meaningful sensitivity experiments.

This long time scale for reaching statistical steadiness is probably a consequence of the long time it takes slowly-settling drizzle-drops to "infect" the depth of the cloud-subcloud layer (see Figs. 1g and h). Again, however, the long delay before drizzle drops are evident in the sub-cloud layer may be alternatively due to the realistic evolution of the cloud itself, or a transient response of the system of equations governing the simulation.

Figure 2a,b illustrate the domain-average behavior of the 6 aerosol bins in the sub-cloud layer (Fig. 2a) and the cloud layer (Fig. 2b). In the sub-cloud layer, bins 1 and 2 are little affected by the formation of the cloud. Bins 3, 4, and 5 exhibit considerable depletion by 200 s, as these particles are swept up into the cloud layer where they are removed by nucleation scavenging. Sub-cloud aerosol in the lowest activation supersaturation (Bin 6), actually increase after an hour, presumably due to the evaporation of droplets which recharge this bin.

In the cloud layer, only Bin 1 remains little affected by nucleation scavenging. All lower activation bins are severely impacted by droplet activation.

b. Three-dimensional fields

The topography of cloud top at 200 min is illustrated in Fig. 3 by displaying the liquid water content surface greater than 0.02 g/kg. The cloud top is hardly uniform, with well-defined hummocks, mesas, and valleys across the domain. These irregular features are

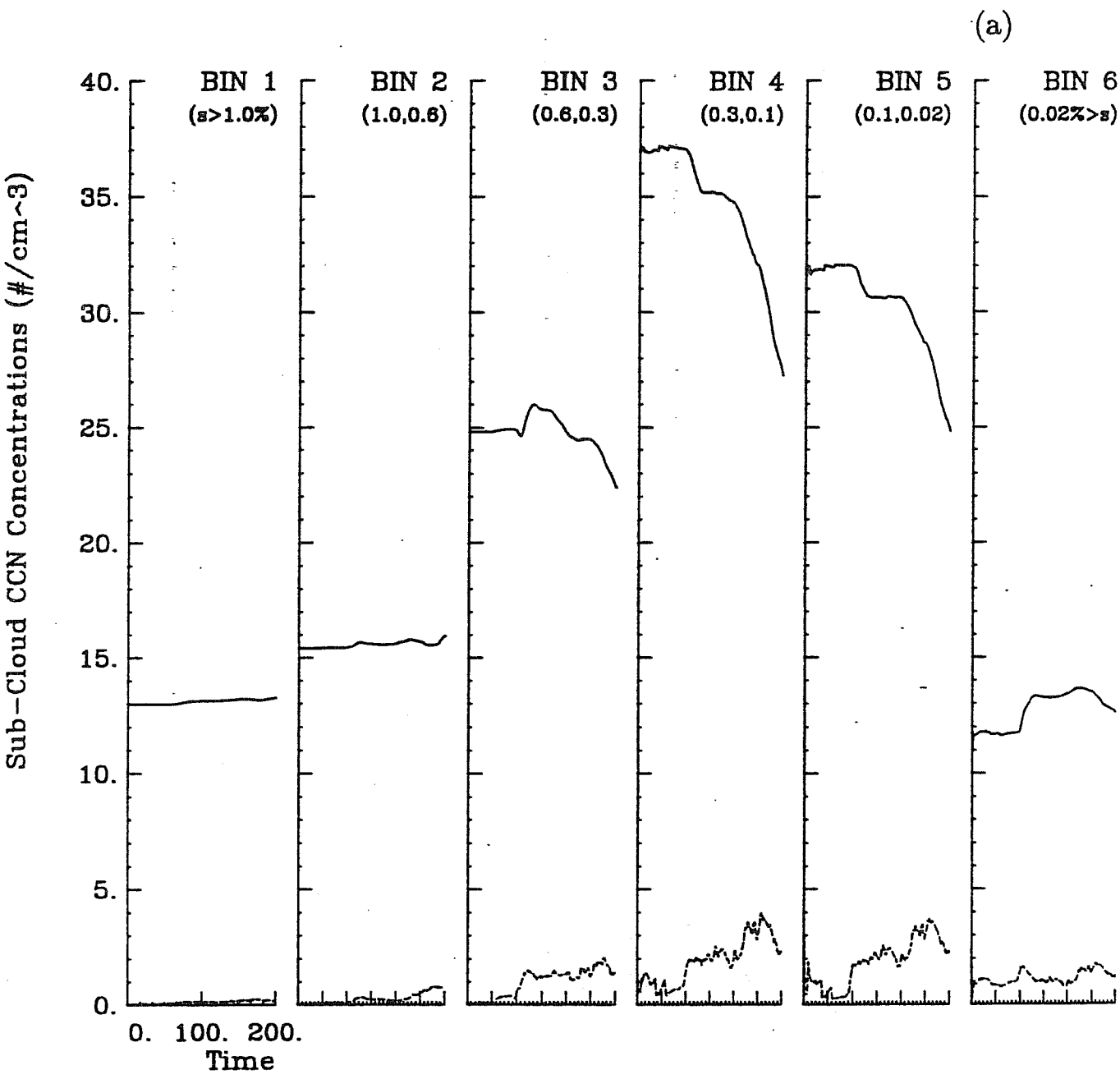

Figure 2: Same as Figure 1, but for sub-cloud CCN concentrations (a); and in cloud CCN concentrations (b).

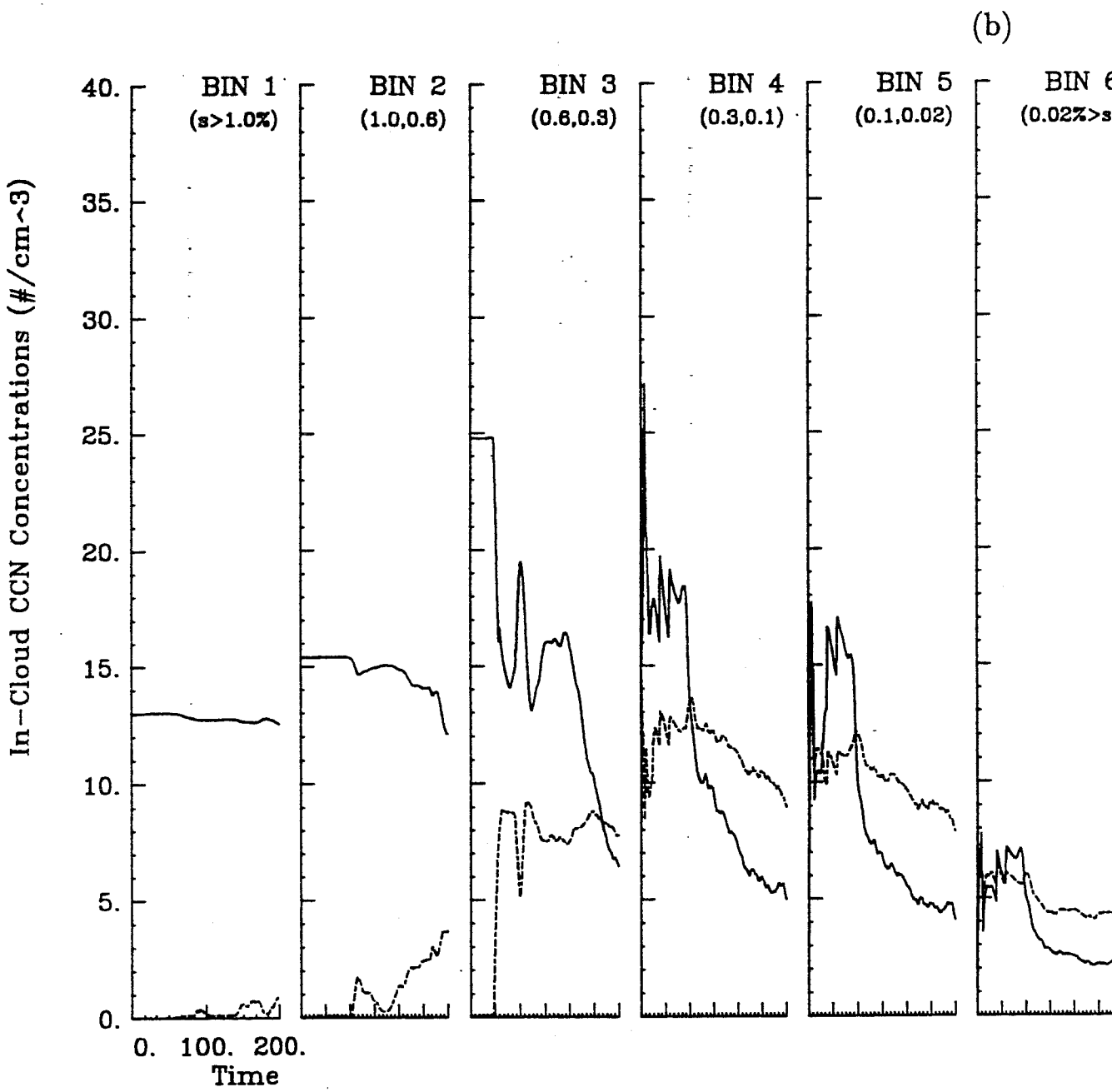

Figure 2: Continued.

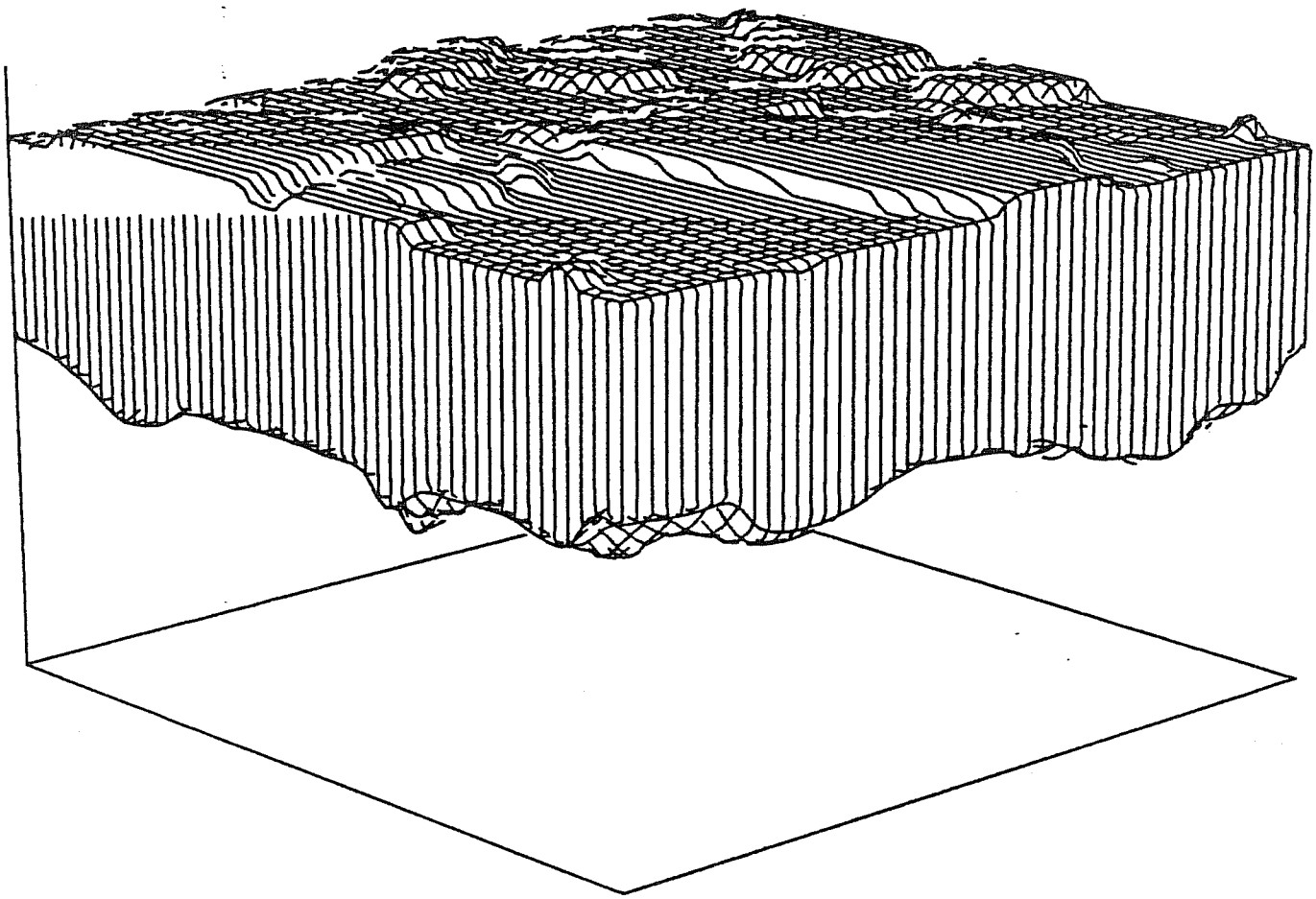

Figure 3: Plot of the 0.02g/kg liquid water surface at 200 minutes; looking down at cloud top. Vertical line in left corner denotes the (x = -1403,y=-1403) point.

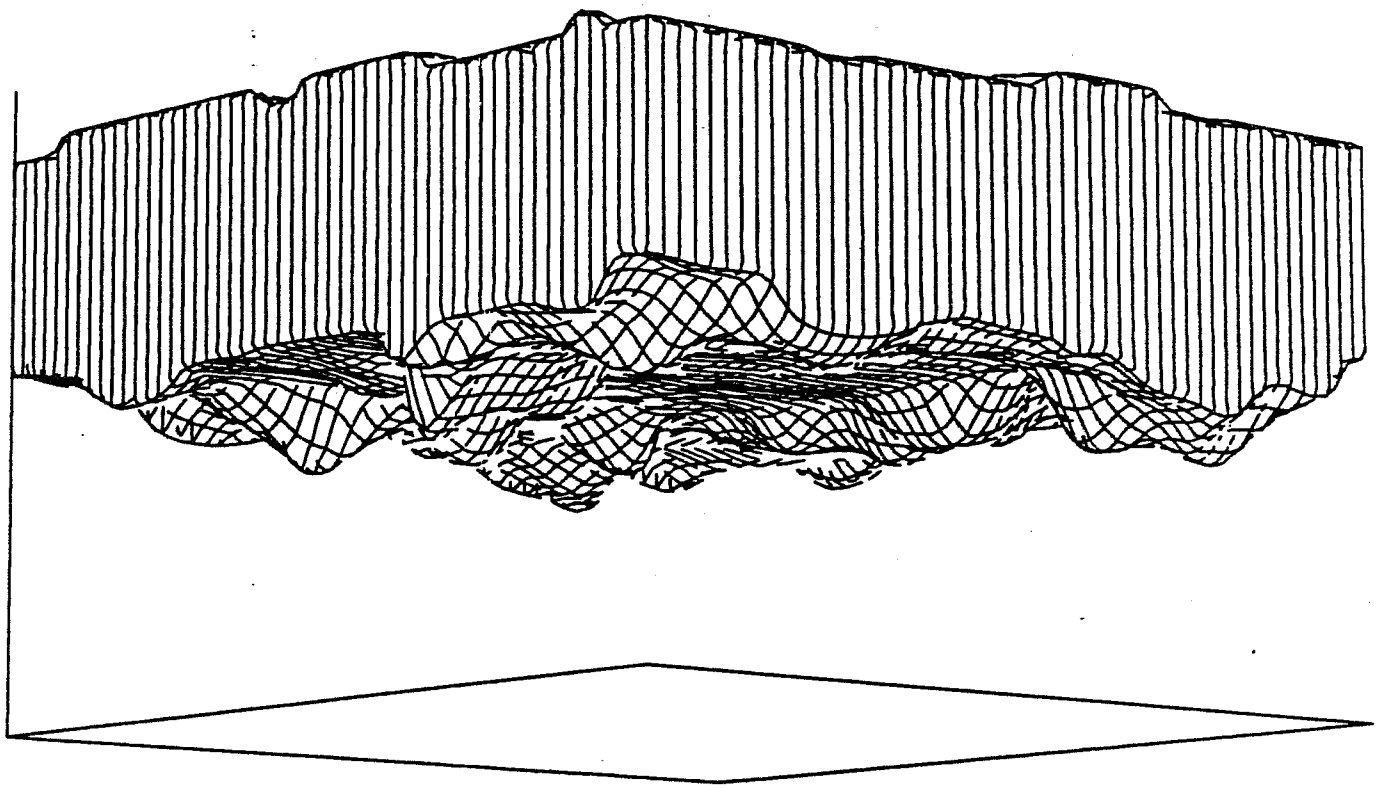

Figure 4: As in Figure 3 but looking up at cloud base.

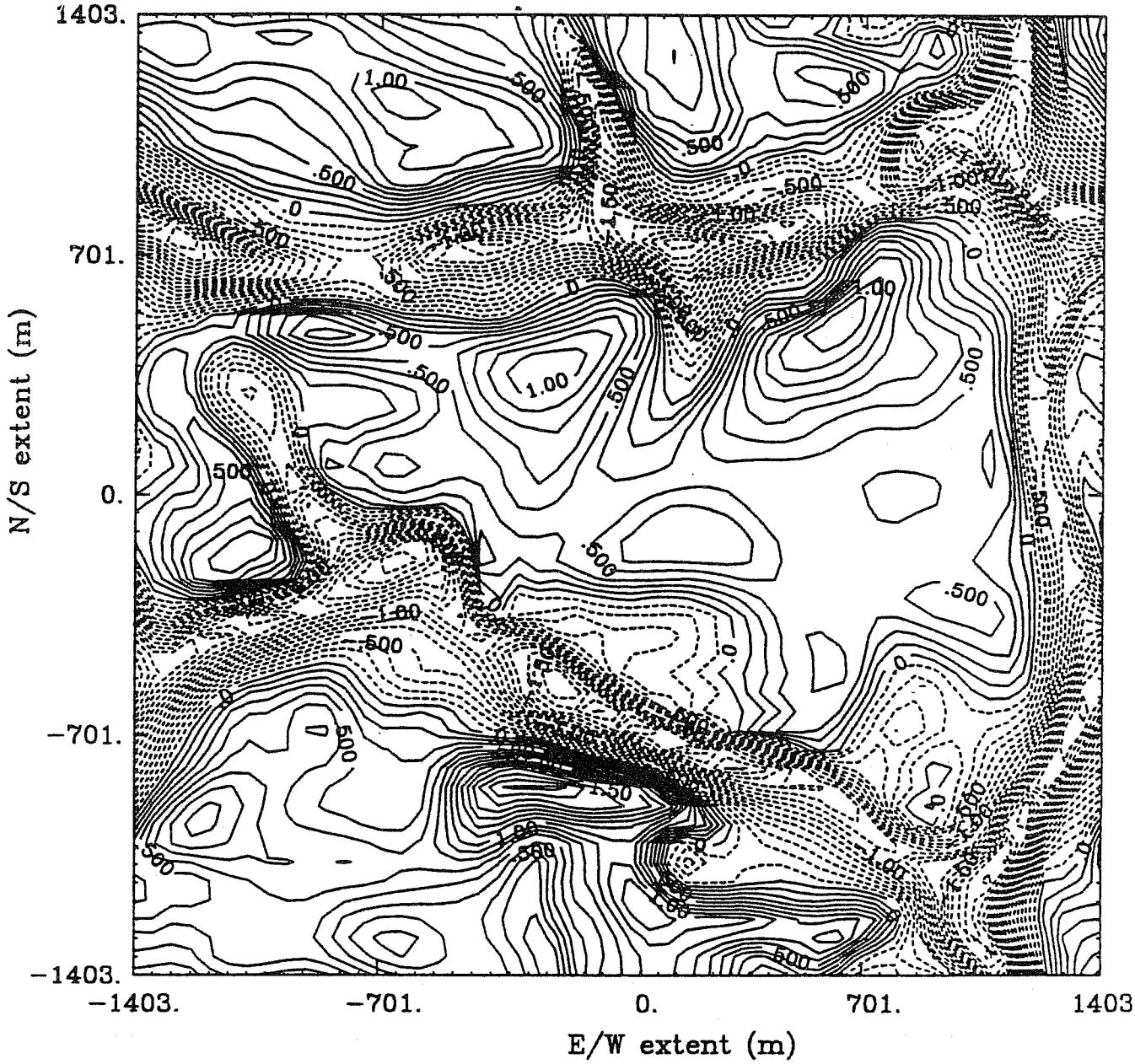

Figure 5: Vertical velocities above cloud base (587 m) at 200 minutes. Negative values given by dashed lines, contour interval 0.125 m/s.

anticipated to significantly alter the albedo of the cloud layer from that found in simple two-stream radiation calculations.

Likewise, cloud base, shown in Fig. 4 is also quite irregular, a feature that is commonly observed off the coast of California (Noonkester, 1984).

The vertical velocity field at 587 m and 200 min is illustrated in Fig. 5. This field, somewhat above cloud base, exhibits a central region of ascent with cells having magnitudes of 0.5 to 1.0 m/s. Surrounding this cell is a sheath of descending air, also in the 0.5 to 1.0 m/s range with other paths of ascent further out from the center.

North-south vertical cross sections at $\pm$ 701 m shows the vertical structure of the cells. Particularly interesting is the rotor-like circulation between 500 to 700 m in the i = 40 cross section. This is air descending from cloud top that gets caught up in a region of updraft.

Particularly important for radiation calculations is the variability of liquid water path (see Fig. 7 which mirrors the variability of the cloud top topography shown in in Fig. 3. We anticipate major differences between radiances and albedo calculated with these fields and those calculated assuming a horizontally uniform cloud layer.

c. *Vertical profiles of horizontally-averaged fields*

We now examine vertical profiles of variables that are averaged across the entire domain (solid line), in updrafts (dashed line), and in downdrafts (dot-dashed). Figure 8 illustrates the average liquid water content vertical profiles. All fields exhibit a generally linear increase in liquid water content with height to maximum values slightly over 0.5 g/kg. The updraft profile exhibits sharp $2\Delta z$ variability near cloud top that is a numerical artifact caused by the sharp gradients in that region. This feature is aggravated, somewhat, by the Tremback et al./Bott sixth-order non-monotonic advection scheme. By using a second order scheme and running from a history file for the last five minutes we are able to significantly dampen the $2\Delta z$ variability near cloud top. Similarly by enhancing subgrid diffusion we expect to be able to dampen this effect. Unfortunately neither of these alternatives are particularly desirable as they don't address the supposed source of the feature (*i.e.*, the non-monotonic

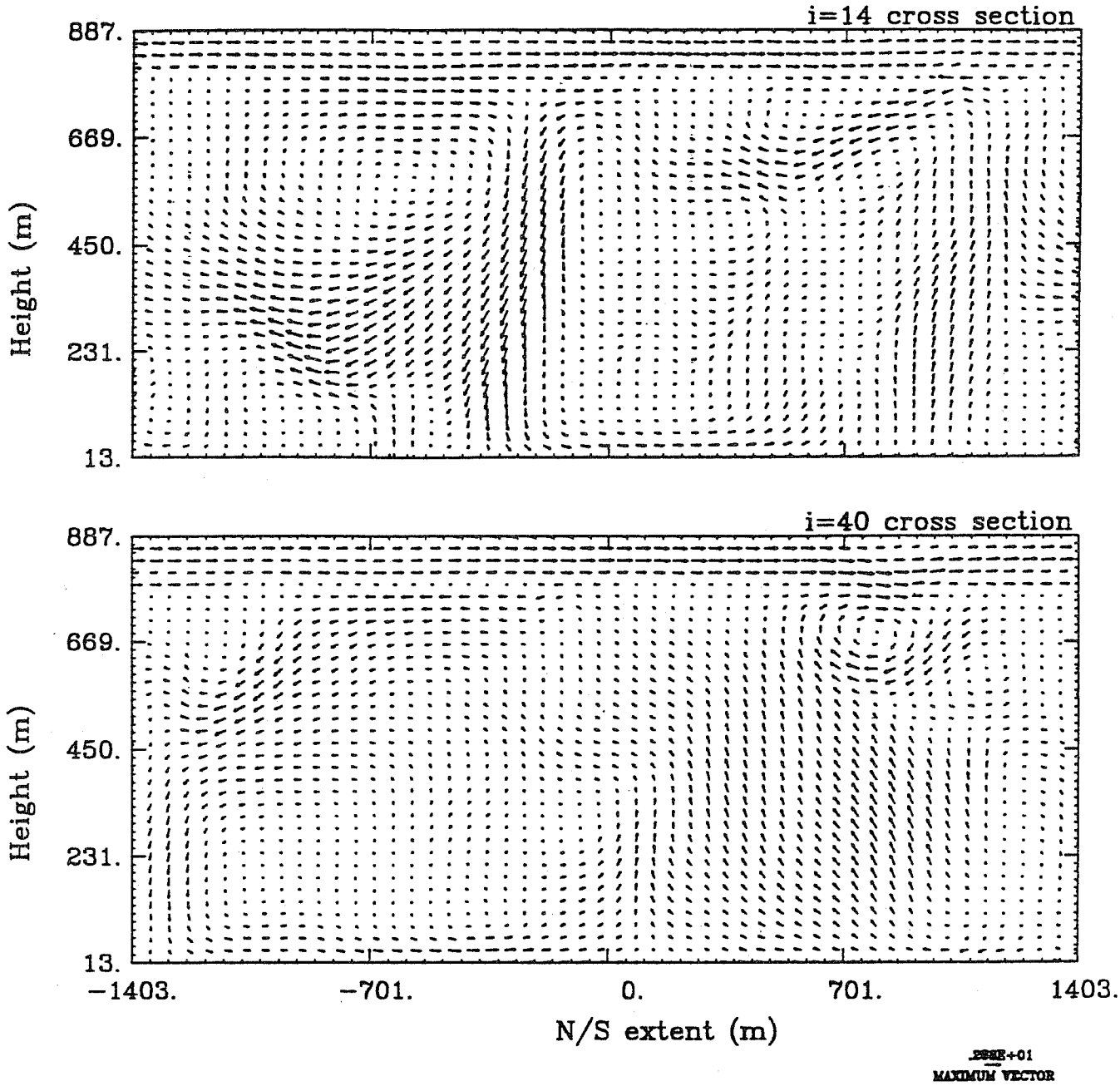

Figure 6: Relative wind vectors in plane of cross sections at 200 minutes. Cross sections taken at $x = -701$ m (i=14) and at $x = 701$ m (i=40). Mean wind subtracted from horizontal winds so wind vector scaling better represents relative circulations.

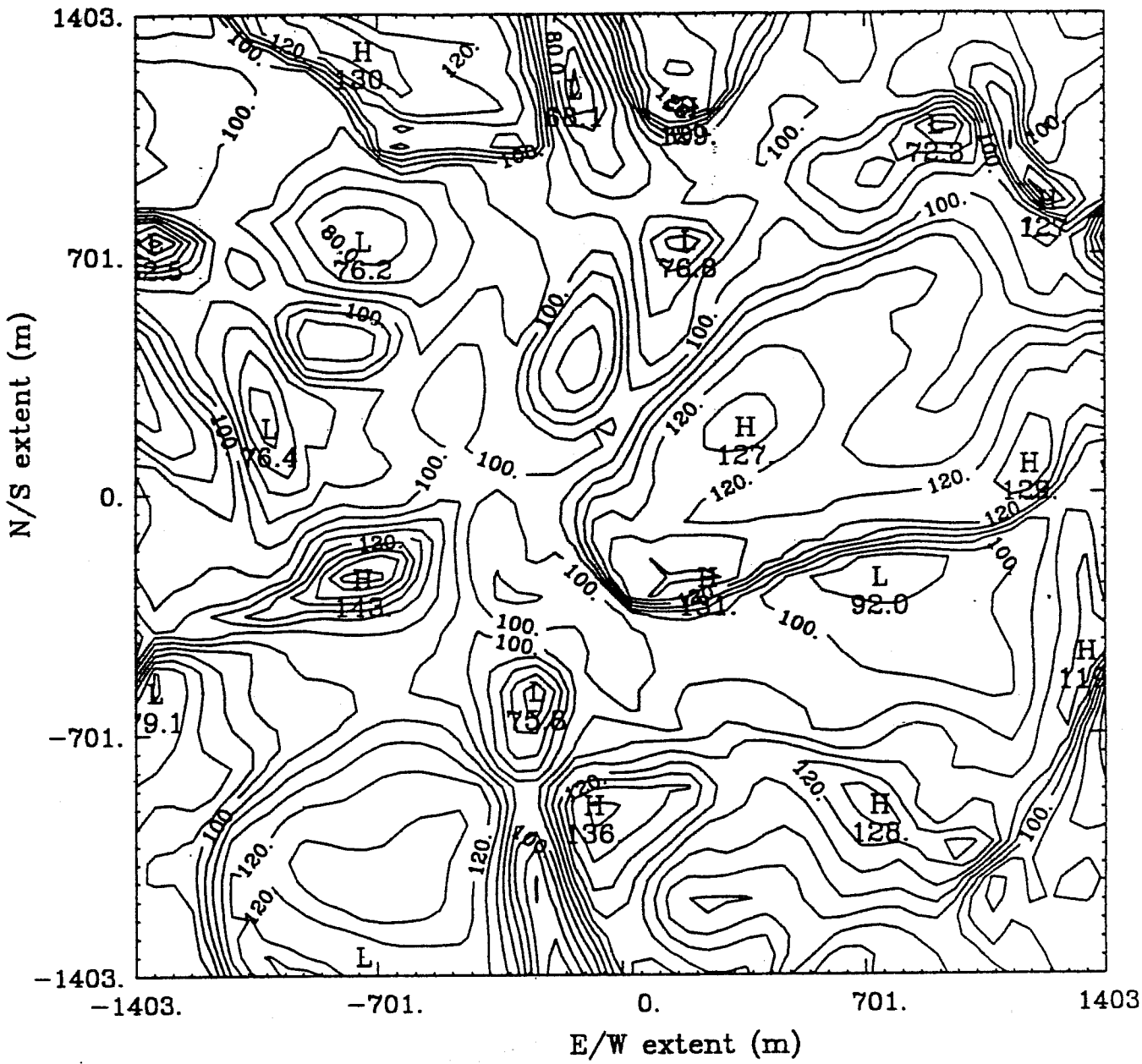

Figure 7: Vertically integrated liquid water paths at 200 minutes. Minimum of 62.5 gm^{-2} at approximately (-1400m, 700m). Maximum of 143 gm^{-2} at approximately (-701m, -300m). Contour interval of 5 gm^{-2}. Solid line is a layer average, dashed line an updraft average, dash-dot line is downdraft average.

nature of the advection scheme). It is hoped that implementation of the monotonic flux corrections of Bott (1992) will mitigate this numerical mode in a physically consistent manner.

Supersaturations in updrafts (Fig. 9) exhibit a rapid rise near cloud base to approximately 0.5% and then decrease with height through most of the cloud layer in accordance with classical theory. Again near cloud top, a $2\Delta Z$ overshoot to over 1% supersaturation can be seem. While there may be a real physical forcing of higher supersaturations near cloud top, since they are greatest in the presence of drizzle scavenging of numerous small droplets, the actual magnitudes is not a resolvable feature.

Figure 10 illustrates that following nucleation near cloud base, droplet concentrations remain nearly constant at about 80 cm^{-3}. The concentrations are somewhat higher in updrafts, approaching 90 cm^{-3} and, not surprisingly, lower in downdrafts. Again, the suspected numerical artifact near cloud top produces concentration of $\sim$ 100 cm^{-3}.

The average effective radius shown in Fig. 11 exhibits a sharp increase to $\sim$11 μm above cloud base, then decreases rapidly, followed by a gradual, nearly linear increase to near cloud top. The largest effective radii are found in downdrafts which are transporting drizzle drops to lower levels.

Small CCN (S > 0.6% activation) concentrations shown in Fig. 12 remain constant through the sub-cloud layer and exhibit a modest linear decrease up to cloud top. The spurious supersaturation near cloud top scavenges the smaller aerosol substantially in that region. Large CCN (S < 0.6%) concentraitons (shown in Fig. 13), on the other hand, are greatly reduced throughout the cloud layer. Contrary to previous suggestions on our part (Cotton, *et al.*, 1992) peak values of large CCN near 800 m (see Fig. 13 have been shown in 2-D sensitivity tests to be largely the result of a numerical mode associated with non-monotonic advection. The possibility of CCN enhancement above cloud top resulting from the evaporation of cloud droplets which recharge the large aerosol bins is still plausible, unfortunately quantifying this effect in our simulations first requires a better treatment of advection. Beneath cloud base the updrafts exhibit a 2 Δz wiggle which is caused by the

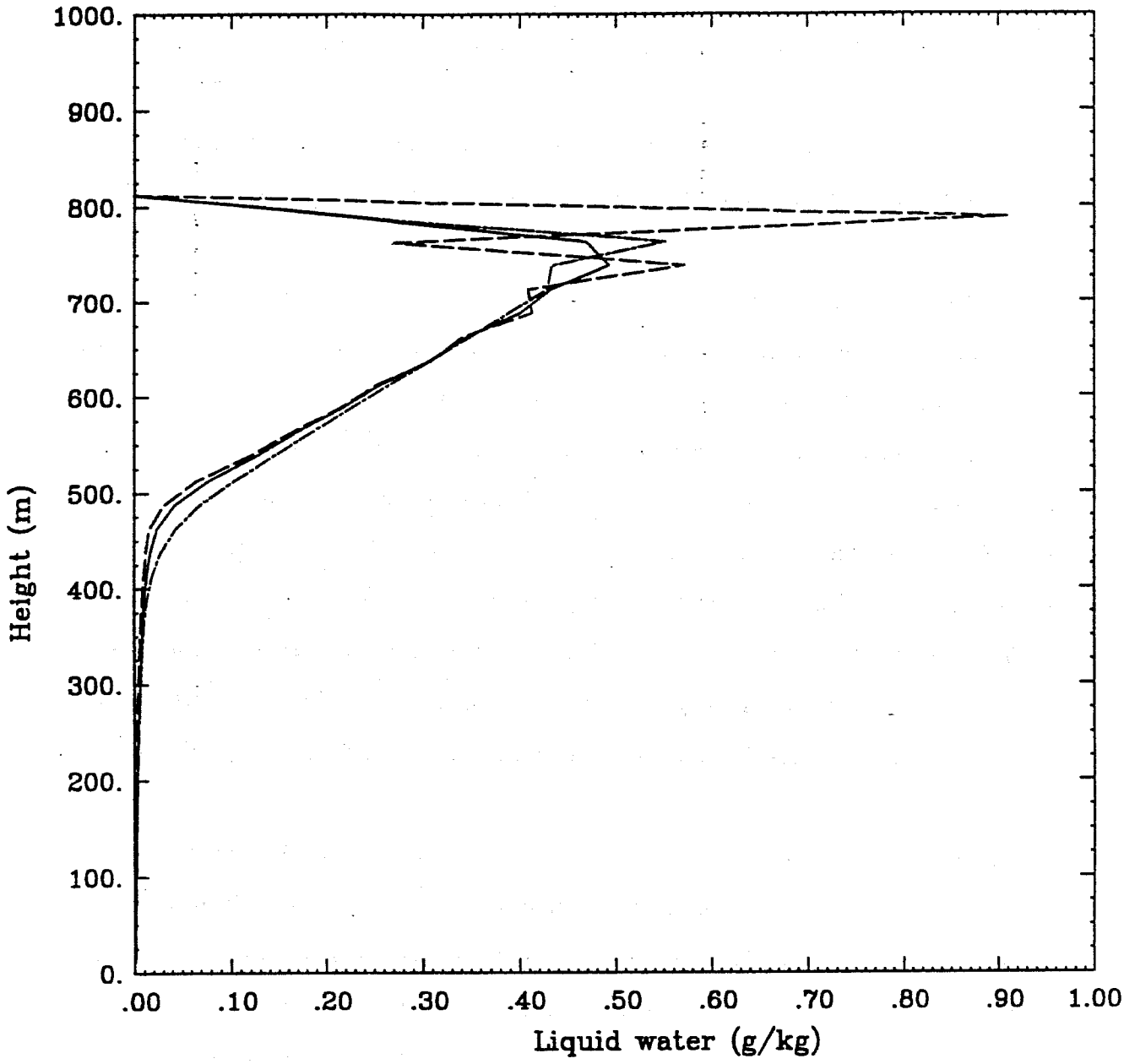

Figure 8: Vertical profiles of liquid water content at 200 minutes. Line designations as in Figure 7.

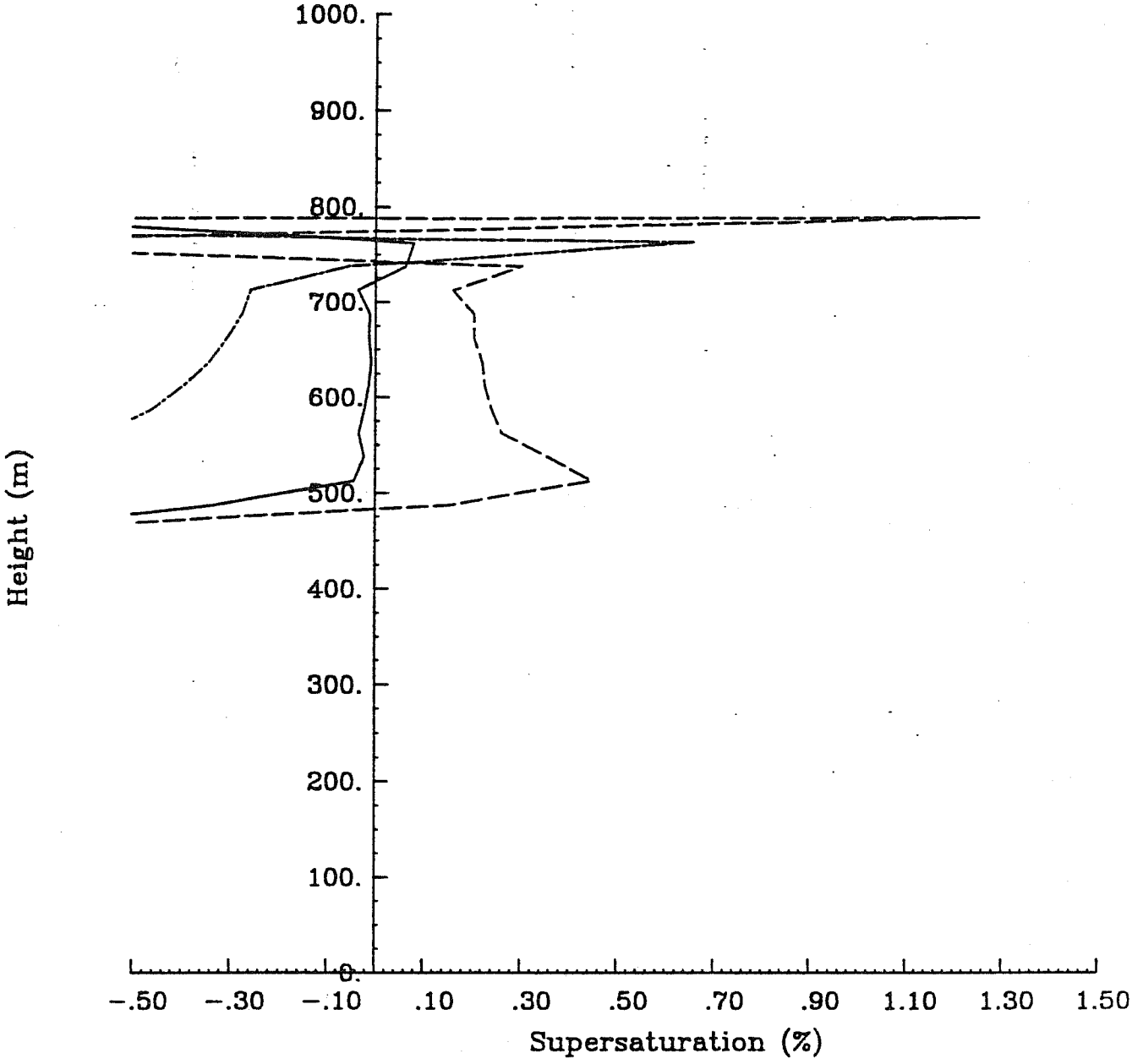

Figure 9: Vertical profiles of supersaturations after 200 minutes. Line designations as in Figure 7.

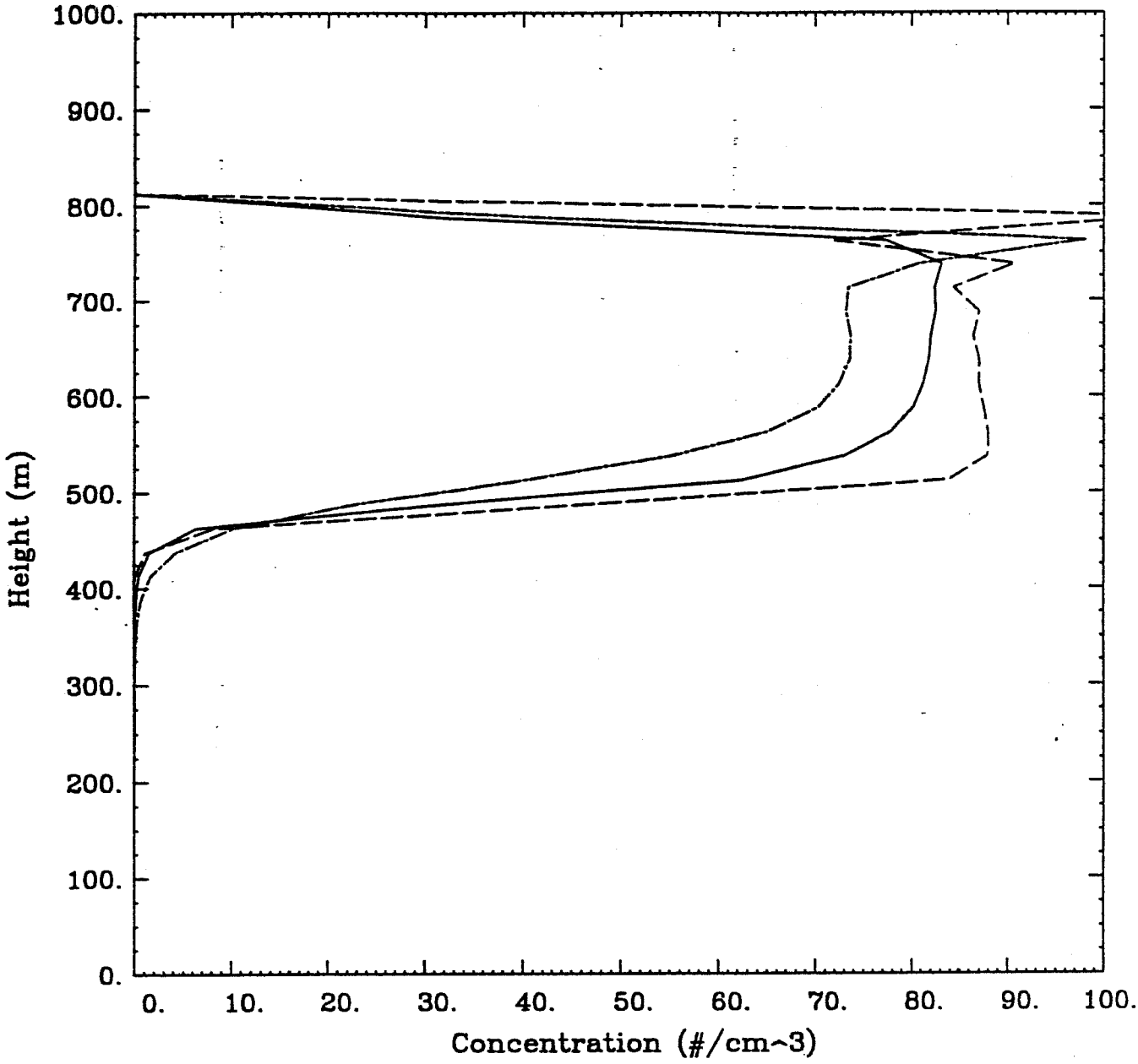

Figure 10: Vertical profiles of number concentrations after 200 minutes. Line designations as in Figure 7.

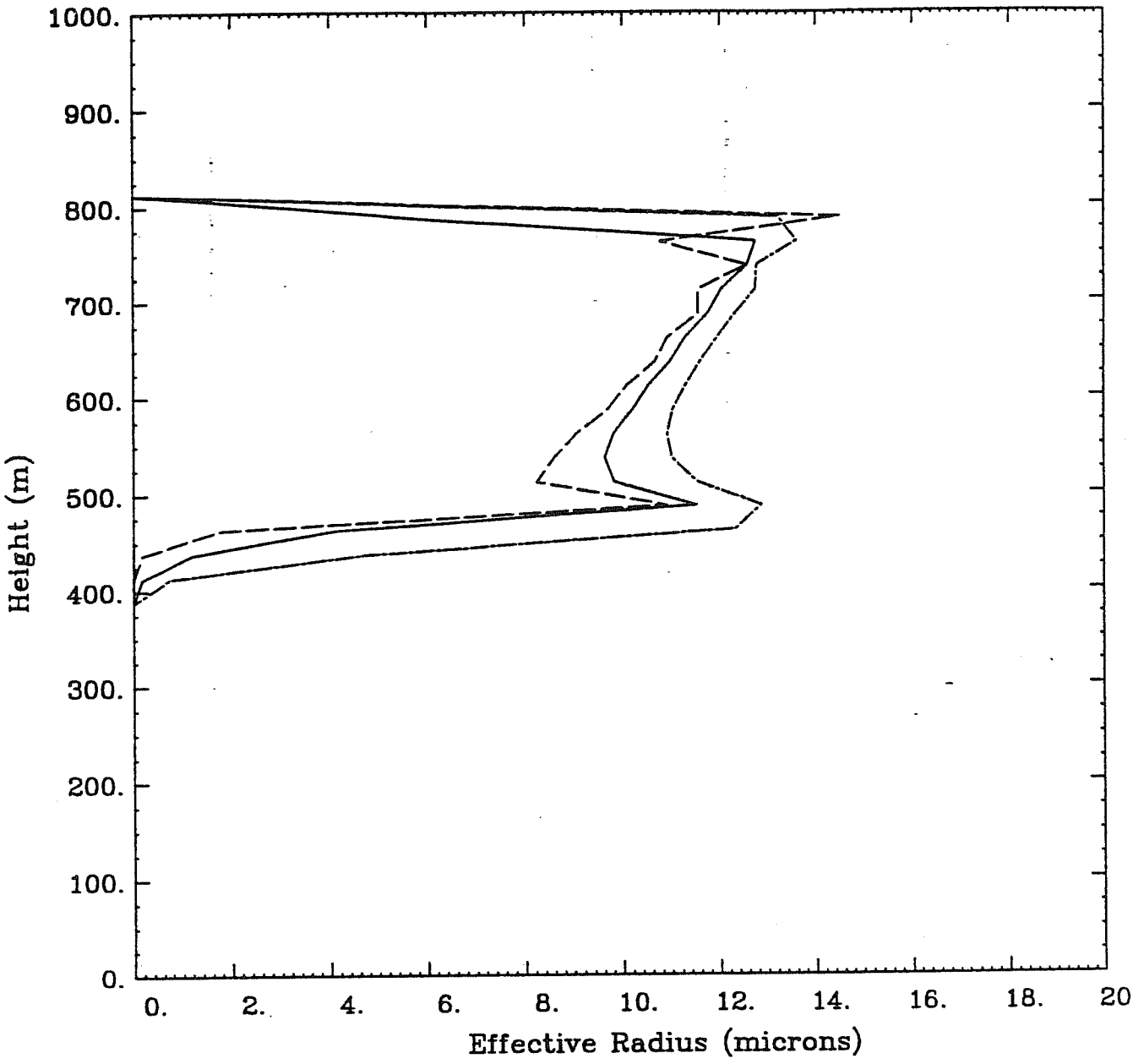

Figure 11: Vertical profiles of effective radius in microns after 200 minutes. Line designations as in Figure 7.

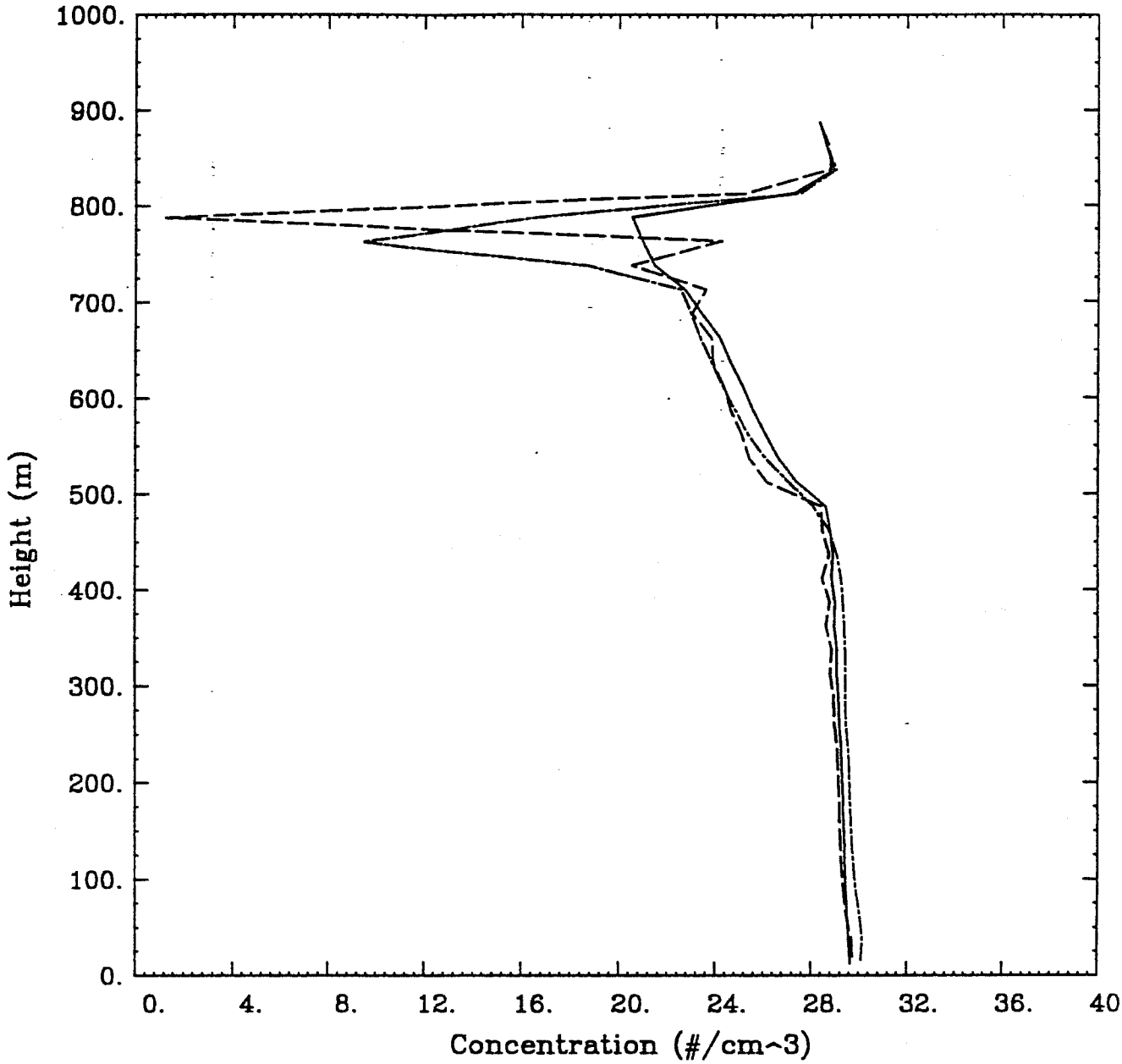

Figure 12: Vertical profiles of small CCN–those which will activate at supersaturations greater than 0.6 % (*i.e.*, bins 1 and 2)–at 200 minutes. Line designations as in Figure 7.

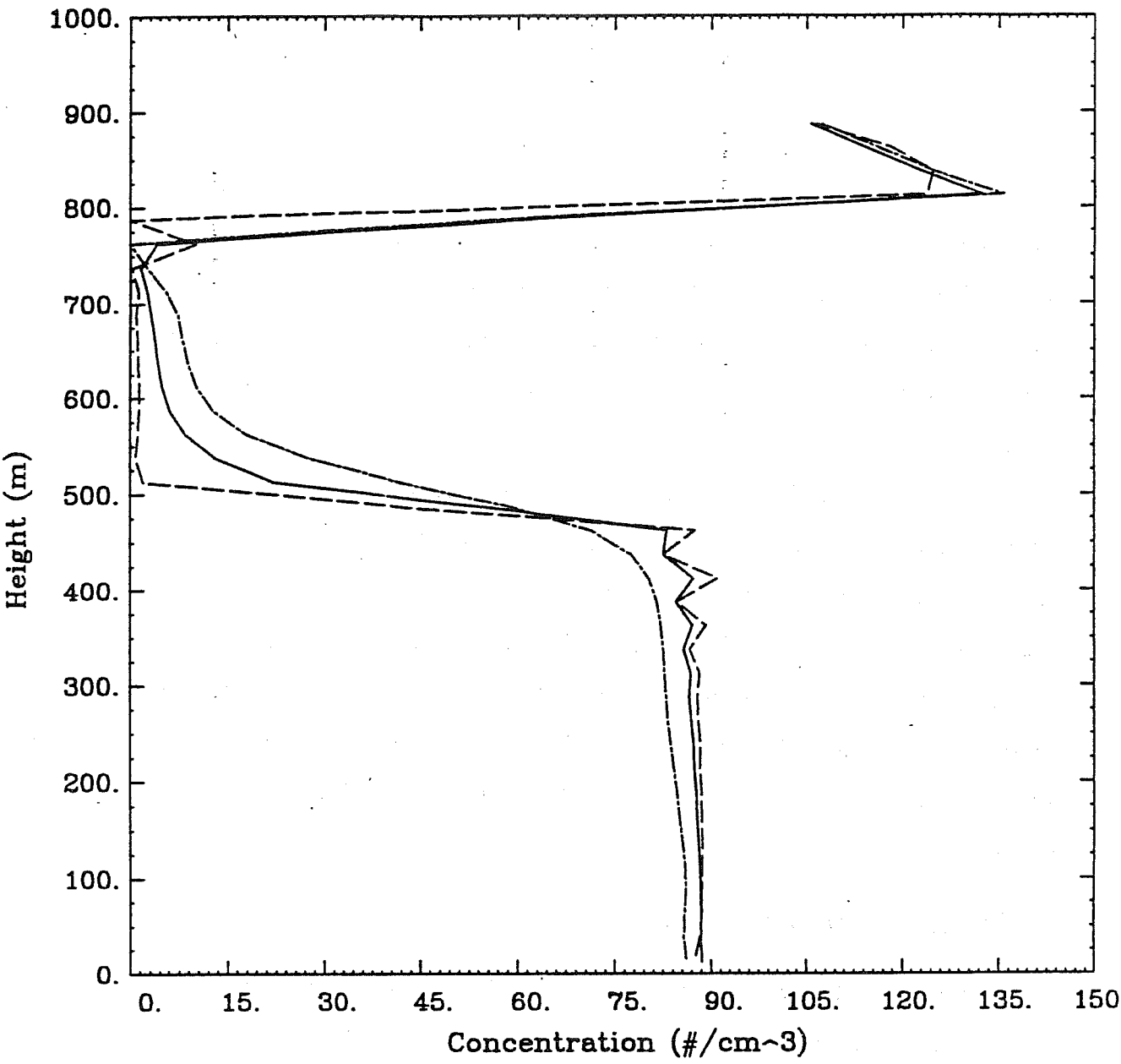

Figure 13: As in previous figure but for large CCN–those which activate at positive supersaturation less thatn 0.6 % (*i.e.*, bins 3-6).

abrupt transition from nearly constant values of the order of 90 cm^{-3} beneath cloud base to near zero at the first cloud grid point.

One of the goals of these modelling studies is to develop a parameterization for stratocumulus clouds based on closure models of a cloud-topped boundary layer (*i.e*, Weissbluth and Cotton's 2.5w scheme). In such a parameterization we hope to base droplet concentrations, cloud depth and liquid water contents on cross correlations between vertical velocity variance, relative humidity, and hygroscopic aerosol abundance. The temporal variation of the maximum layer-averaged vertical velocity variance is well correlated with the domain averaged w_{RMS} plotted in fig. 1, which in turn appears to be well correlated to supersaturations and liquid water contents.

In Fig. 14 the vertical velocity variance is plotted throughout the boundary layer. At this time (as well as all other times examined) the downdrafts dominate. In addition at 200 minutes we see the downdraft vertical velocity variance is rather symmetric with a maximum in the lower cloud through sub-cloud region. The updraft vertical velocity exhibits a relative minimum just below cloud base, with relative maximums in the lower levels. All the profiles decrease rapidly to null values at cloud top. The layer averaged vertical velocity diminishes to half its maximum value approximately mid way through the cloud and approaches its extremum assymptotically.

d. Droplet spectra and drizzle

Simulated droplet spectra shown in Fig. 15 at 362 m to 762 m are shown at 200 min. Because this is at a time when drizzle has "infected" the entire depth of the cloud layer, the droplet spectra are particularly broad (although the scaling of the graphs with 9 orders of magnitude in the vertical exaggerates this feature considerably), especially the mass spectra (short dashed line). The pronounced 10 μm mode is clearly evident in cloud (upper three levels of plots), while not evident in the sub-cloud spectra plots (Note: cloud base is predominantly above the 462 m level.)

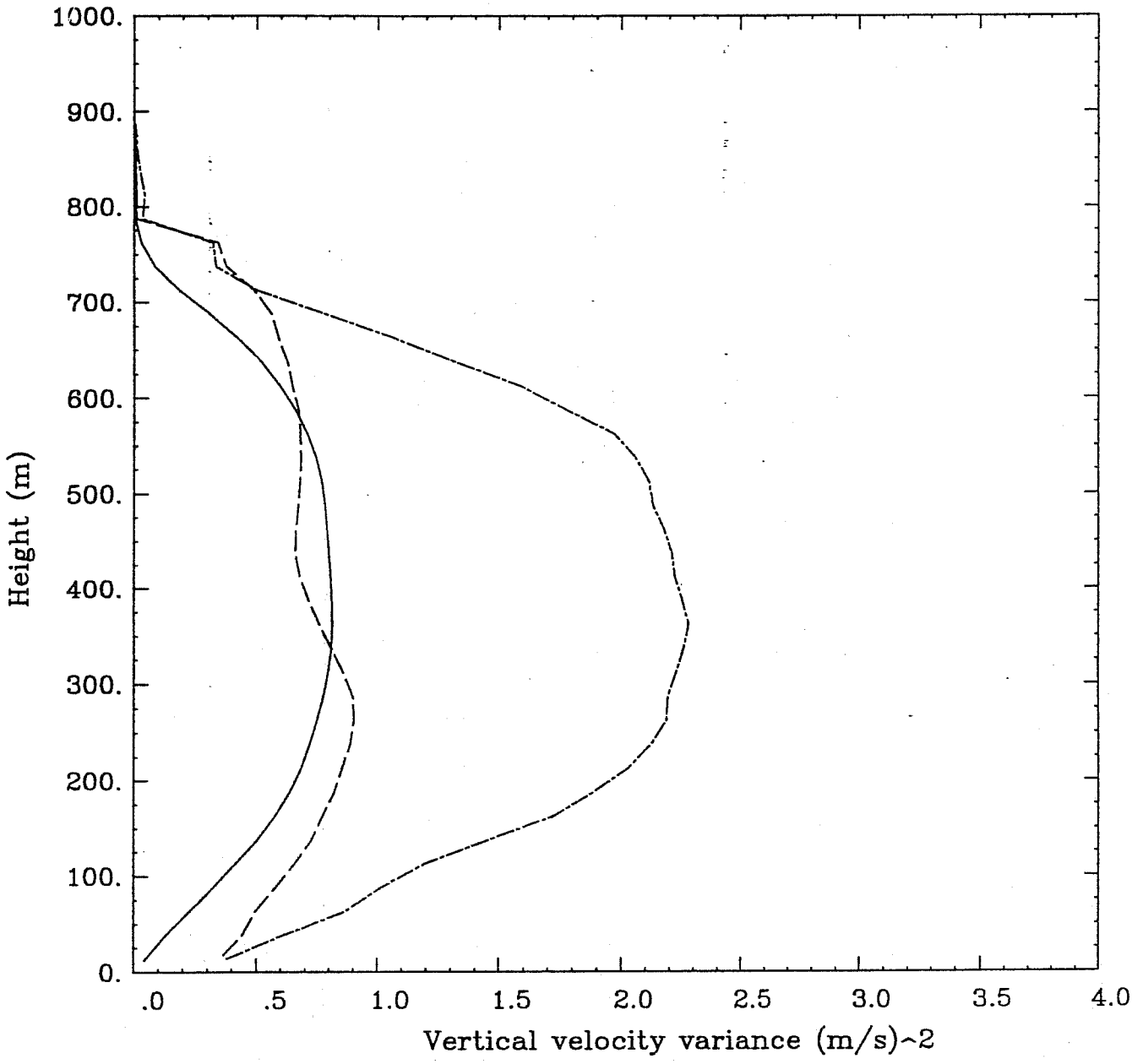

Figure 14: Vertical profiles of vertical velocity variance at 200 minutes.

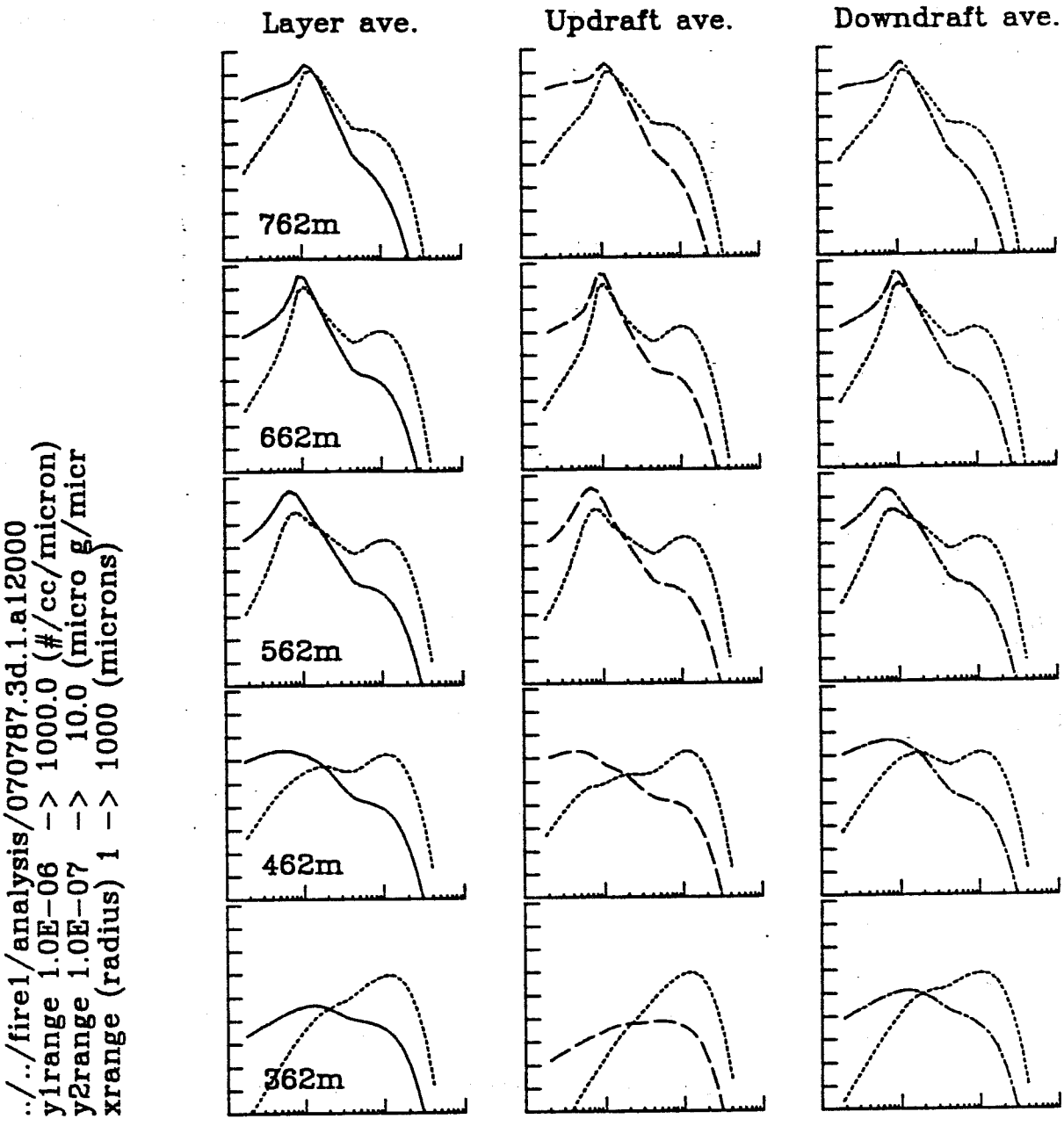

Figure 15: Droplet spectra for five different levels after 200 minutes. Short dashed lines represent mass spectra. Abscissa from 1 micron to 1 mm logrithimically. Ordinate from $10^{-6} \rightarrow 10^{3} \#cm^{-3}\mu m^{-1}$ for number representation, from $10^{-7} \rightarrow 10^{2} \mu g cm^{-3}\mu m^{-1}$ for mass distribution.

The surface drizzle rate, shown in Fig. 16, is quite patchy and resembles the surface precipitation mappings expected from deep cumulus convection. The magnitudes differ substantially from deep convection, however, with peak values being only 9 μm/hr! Likewise, the accumulated surface precipitation for the entire 3 hr simulation period is only 7.3 μm!

5. Summary and Conclusions

Our first three-dimensional LES/explicit microphysics simulation of a marine stratocumulus cloud layer with RAMS has been conducted. Results of the simulation are consistent with observations of stratocumulus clouds off the California Coast including nearly constant droplet concentrations through most of the cloud layer, liquid water contents and droplet effective radii that increase linearly with height through the cloud layer, and supersaturations that remain below 0.15%.

The only departure from reality is at grid points near cloud top where supersaturations of the order of 1.3% and droplet concentrations about 20% above typical cloud values are found. These anomalies are believed to be numerical artifacts resulting from non-monotonic advection.

Nonetheless, the pronounced horizontally-varying fields of cloud macrostructure and microstructure should be useful for applying 3D radiation codes to examining the impacts of such variability on cloud radiances and albedo. Care must be taken, however, in removing cloud top grid points from the analysis.

Likewise, the simulated data should be useful in testing closure models of a cloud-topped boundary layer such as Weissbluth and Cotton's (1993) level 2.5w scheme. Moreover, one could examine potential extensions of the scheme to include activation (scavenging) of CCN spectra as a function of vertical velocity variance.

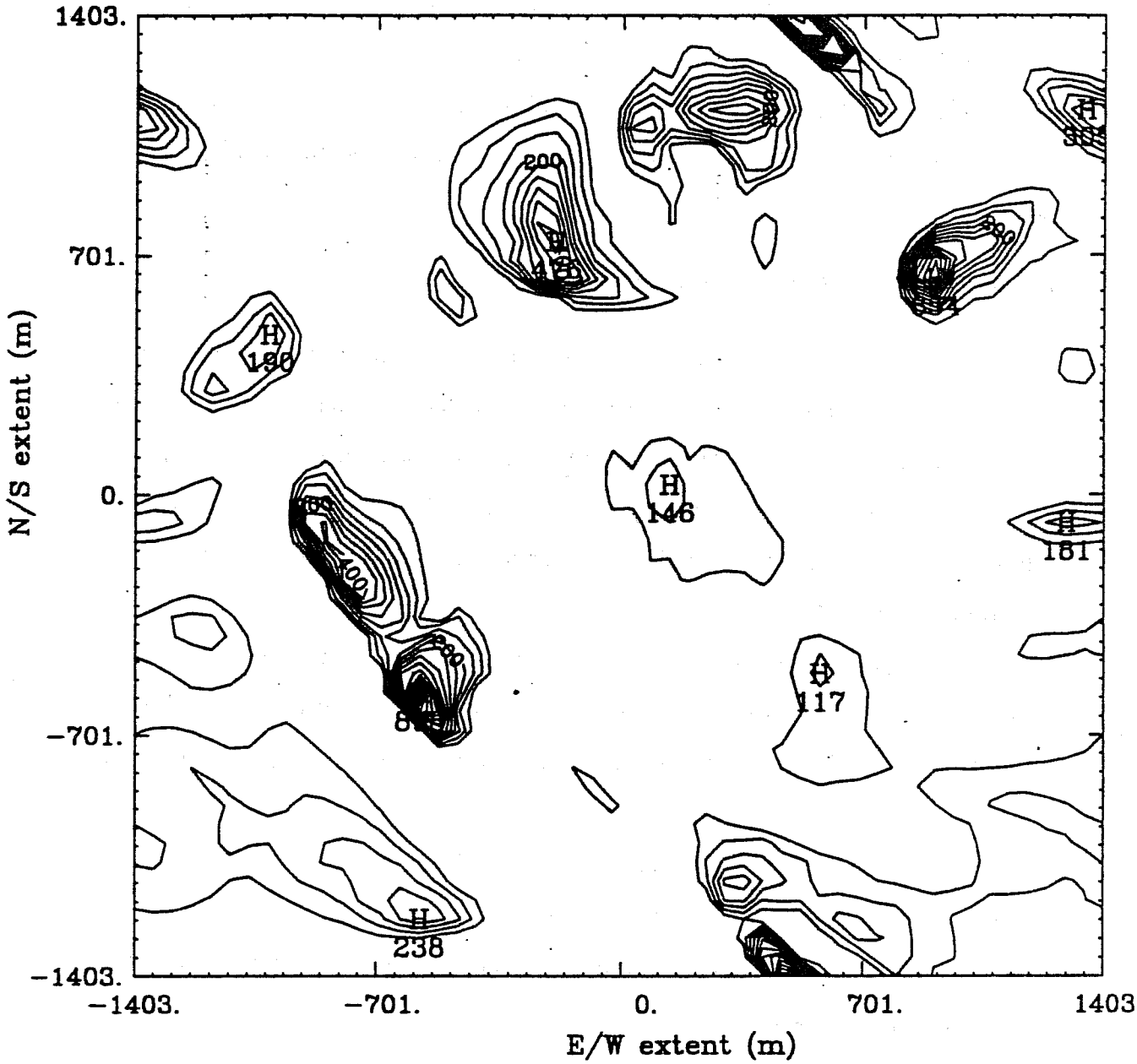

Figure 16: Rain rate at surface at 200 minute point. Contours at intervals of 0.5 microns per hour.

6. Acknowledgements

Thanks are given to Brenda Thompson in processing the manuscript. William Cotton thanks the World Meteorological Organization and GCSS for providing travel support for this meeting. This research was supported by Research Agreement Number NIGEC-91-S01 from the U.S. Department of Energy through the National Insititute for Global Environmental Change.

References

Albrecht, B.A., 1989: Aerosols, cloud microphysics, and fractional cloudiness. *Science,* **245,** 1227-1230.

Betts, A.K., and R. Boers, 1990: A cloudiness transition in a marine boundary layer. *J. Atmos. Sci.,* **47,** 1480-1497.

Bleck, R., 1970: A fast approximative method for integrating the stochastic coalescence equation. *J. Geophys. Res.,* **75,** 5165-5171.

Bott, A., 1989: A positive definite advection scheme obtained by nonlinear renormalization of the advective fluxes. *Mon. Wea. Rev.* **117,** 1006-1015

Bott, A., 1992: Monotone flux limitation in the area-preserving flux-form advection algorithm. *Mon. Wea. Rev.* **120,** 2592-2602

Charlson, R.J., S.E. Schwartz, J.M. Hales, R.D. Cess, J.A. Coakley, Jr., J.E. Hansen, D.J. Hofmann, 1992: Climate forcing by anthropogenic aerosols. *Science,* **255,** 423-430.

Chen, C. and W.R. Cotton, 1983: Numerical experiments with a one-dimensional higher order turbulence model: Simulation of the Wangara Day 33 Case. *Boundary-Layer Meteorol.,* **25,** 375-404.

Cotton, W.R., G.J. Tripoli, R.M. Rauber and E.A. Mulvihill, 1986: Numerical solution of the effects of varying ice crystal nucleation rates and aggregation processes on orographic rainfall. *J. Climate. Appl. Meteor.*, **25**, 1658-1680.

Cotton, W.R., B. B. Stevens, G. Feingold and R. L. Walko, 1992: A model for simulating the Twomey effect. *Report to the Third WMO Cloud Modelling Workshop*, Toronto, August 1992.

Feingold, G., S. Tzivion, and Z. Levin, 1988: Evolution of raindrop spectra. Part I: Solution to the stochastic collection/breakup equation using the method of moments. *J. Atmos. Sci.*, **45**, 3387-3399.

Flatau, P.J., R.L. Walko, and W.R. Cotton, 1992: Polynomial fits to saturation vapor pressure. *J. Appl. Meteor., in press.*

Hadfield, M.G., W.R. Cotton, and R.A. Pielke, 1991: Large-eddy simulations of thermally forced circulations in the convective boundary layer. Part I: A small-scale, circulation with zero wind. *Boundary-Layer Meteorol.*, **57**, 79-114.

Hadfield, M.G., W.R. Cotton, and R.A. Pielke, 1992: Large-eddy simulations of thermally forced circulations in the convective boundary layer. Part II: The effect of changes in wavelength and wind speed. *Boundary-Layer Meteorol.*, 58, 307-327.

Hudson, J.G., and P.R. Frisbie, 1991: Cloud condensation nuclei near marine stratus. *J. Geophys. Res.*, **96**, 20,795-20,808.

Johnson, D.B. 1980: The role of giant and ultragiant aerosol particles in warm rain initiation. *J. Atmos. Sci.*, **39**, 448-460.

Louis, J.F., 1979: A parametric model of vertical eddy fluxes in the atmosphere. *Boundary-Layer Meteorol.*, **17**, 187-202.

Mitra, S.K., H.R. Pruppacher and J. Brinkmann, 1992: A windtunnel study on the drop-to particle conversion. *J. Aerosol Sci.*, **23**, 245-256.

Noonkester, V.R., 1984: Droplet Spectra Observed in Marine Stratus Cloud Layers. *J. Atmos. Sci.*, **41**, 829-844.

Tremback, C.J., J. Powell, W.R. Cotton and R.A. Pielke, 1987: The Forward-in-Time Upstream Advection Scheme: Extension to Higher Orders. *Mon. Wea. Rev.*, **115**, 540-555.

Tripoli, G.J., and W.R. Cotton, 1981: The use of ice-liquid water potential temperature as a thermodynamic variable in deep atmospheric models. *Mon. Wea. Rev.*, **109**, 094-1102.

Twomey, S., 1974: Pollution and the planetary albedo. *Atmos. Environ.*, **8**, 1251-1256.

Twomey, S., 1977: The influence of pollution on the short wave albedo of clouds. *J. Atmos. Sci.*, **34**, 1149-1152.

Twomey, S., 1959: The nuclei of natural cloud formation: the supersaturation in natural clouds and the variation of cloud droplet concentrations. *Geofis. Pura et appl.*, **43**, 243-249.

Tzivion, S., G. Feingold, and Z. Levin, 1987: An efficient numerical solution to the stochastic collection equation. *J. Atmos. Sci.*, **44**, 3139-3149.

Tzivion, S., G. Feingold, and Z. Levin, 1989: The evolution of raindrop spectra. Part II: Collisional collection/breakup and evaporation in a rain shaft. *J. Atmos. Sci.*, **46**, 3312-3327.

Walko, R.L., W.R. Cotton, and R.A. Pielke, 1992: Large eddy simulations of the effects of hilly terrain on the convective boundary layer. *Bound.-Layer Meteorol.*, **53**, 133-150.

Weissbluth, M.J., and W.R. Cotton, 1993: The representation of convection in mesoscale models. Part I: Scheme fabrication and calibration. Accepted *J. Atmos. Sci.*